

Interactive learning environment for diagnostic radiography with real-time X-ray simulation and patient positioning

Aaron Sujar^{a,b,*}, Marcos García^a, Luis Pastor^a, Graham Kelly^{c,b}, Franck P.Vidal^b

^a*Grupo de Modelado y Realidad Virtual, Universidad Rey Juan Carlos, Spain*

^b*Bangor University, United Kingdom*

^c*Shrewsbury and Telford Hospital NHS Trust*

Abstract

Keywords: Real-time simulation, interactive simulation, character animation, interactive learning environment, X-rays, diagnostic radiography

Rewrite abstract right at the end, after feedback from Graham. Use keywords in the abstract

1. Introduction

2 Projectional radiography (also called projection radiography, and X-ray radiography) is a very common medical imaging tool that supports clinicians in the diagnostic
3 of certain diseases, infections, injuries (e.g. bone fractures), and to locate foreign objects. It can be used in almost every part of the patient's body although each specific
4 body location requires a given patient position and X-ray machine set up, in particular
5 collimation of the X-ray source, voltage of the X-ray tube, time of exposure, distance
6 source to patient, and distance source to detector or film.

9 Undergraduate radiographer training within the UK is a mix of academic theory and
10 clinical practice. Trainee radiographers learn theoretical information such as anatomy
11 and radiation physics. Theoretical information is learnt within the classroom setting
12 however, many institutions utilise creative simulations in order for the trainee to experience
13 the clinical environment within a non-clinical setting such as the university. Depending
14 on the university facilities trainees also x-ray phantom anatomy in order to further their
15 understanding of radiation physics principles without the risk of biological damage to
16 living tissue. Trainees can then see the effect of imaging principles such as exposure
17 factors in real time, a practice that could not be performed on living tissue. Teaching
18 cases are utilised within the academic setting again to demonstrate clinical cases. They
19 are compilations of patient histories including their medical images, recorded discussions,
20 notes and annotations. Trainees can then study well-documented cases through
21 large image datasets. University hospitals and medical schools often build their own

*Corresponding author.

Email address: aaron.sujar@urjc.es (Aaron Sujar)

22 repositories. However, there are now more and more online public resources where
23 radiographers can access vast sets of images from any part of the human anatomy [1].

24 Nowadays, digital technologies are more ubiquitous than ever and smartphones
25 start to play a big role in learning. Some institutions have created mobile phone apps
26 in which trainees can look up images, fill in questionnaires, e.g. [UBC Radiology](#) [2].
27 This type of resources are playing an increasing role in the curriculum of trainees in
28 radiology and diagnostic radiography. Nevertheless, all these images show the final
29 results and do not describe the whole procedure. Also, as there are static images, it
30 is not possible to modify any acquisition parameter (e.g. tube voltage) to interactively
31 visualise the changes in the X-ray radiographs corresponding to this parameter modifi-
32 cation. According to the old adage, “we learn from our mistakes”. However, trainees
33 are not allowed any mistake in patients due to the use of ionising radiations. For safety
34 reasons, projections obtained with different set ups never come from the same patient,
35 hindering any possible comparison. Furthermore, patient positioning is a key step and
36 it cannot be easily learned from the final images.

37 [It is a vital aspect of undergraduate training that mistakes are learnt from to ensure](#)
[they are not replicated within the real clinical setting. For trainees to further understand](#)
[errors an x-ray room is required within the academic setting. The use of an anatomical](#)
[phantom is also then required to x-ray in order to demonstrate these errors. This](#)
[cannot be easily conducted within a typical classroom setting and therefore constitutes](#)
[a separate teaching session. This could lead to a disconnect between theory and practice.](#)

43
44 Virtual reality (VR) medical simulation is playing an increasing role in the physi-
45 cians’ curriculum, such as surgeons and other specialists [3, 4]. They are applied to
46 a wide variety of medical procedures [5, 6]. Such applications are used for safe and
47 effective training purposes. Unlike traditional methods (using cadavers, animals or
48 mannequins), computerised simulators permit new physicians to improve and develop
49 their non-cognitive skills in a cheap and safe environment [7]. It is also possible to use
50 such simulators without the close supervision of an expert.

51 Recent advances in computer graphics (CG) allow the development of new simula-
52 tors that can be used in the apprenticeship of radiographers. In this context, it is worth
53 to mention two computerised simulators. On one hand, [8] is a simulator for training in
54 interventional radiology where fluoroscopy (real-time X-ray images) is used to guide
55 a needle towards an anatomical structure. Despite of the fact that the simulator has
56 an interactive X-ray simulation and the deformation of lung tissues, there is only one
57 example of patient and it is only focused on the chest area.

58 On the other hand, ProjectionVR™ is a simulator that immerses the user into a re-
59 alistic 3D X-ray room to simulate the complete procedure [9]. With virtual digitised
60 patient data, it replicates an interactive learning environment without the risk of radi-
61 ation exposure to students or patients. Although it provides a variety of real cases, the
62 greatest limitation of this tool is that users always load the same static images with the
63 same examples and they cannot produce new X-ray images instantly. There are only
64 pre-computed images and users are not able to re-position a particular patient or play
65 with anatomy variations and pathologies. Another simulator, called medspace.VR,
66 provides an immersive 3D environment [10]. Although it allows to modify the patient
67 position, only skin and bones seem to be present in the produced X-ray images and

68 there is a lack of variety in the anatomic models.

69 Patient variability is desirable so that trainees can be exposed to all kind of possibilities, e.g. from underweight to overweight patients, from babies to elderly patients. It
70 is also beneficial for simulators to emulate specific scenarios (e.g. a detecting foreign
71 bodies, or collapsed lung) which would have been difficult to routinely encounter as a
72 student.

73 In this paper, we propose an X-ray projectional radiograph simulator that can be
74 used as an interactive teaching and learning environment where teachers and students
75 are able to review numerous virtual patients with the possibility to manipulate the pa-
76 tient positioning and the X-ray machine parameters in realtime. Our tool was designed
77 with the following requirements in mind:

- 79 • It could use a wide variety of existing virtual patient models.
- 80 • Users can interactively manipulate the virtual patient to the position required in
81 any given procedure.
- 82 • Users can observe the X-ray image immediately as they change the virtual pa-
83 tient's position, X-ray source's position or any other X-ray machine parameter.

84 To fulfil the requirements mentioned above, our simulator is made of three main
85 modules: the Virtual X-ray Imaging Library (gVirtualXRay), the Virtual Patient Posi-
86 tioning System (VPPS) and the courseware. The first one is in charge of generating
87 the X-ray image from a triangular mesh in realtime. This module is able to simulate
88 the most relevant X-ray configuration parameters. VPPS transforms the anatomy of a
89 virtual patient to the desired position. It was designed to be flexible to deal with as
90 many virtual patients as possible. With this goal in mind, our algorithm works with
91 incomplete anatomical models (skin and bones are the minimum tissues required) and
92 the biomechanical properties of the virtual patient tissues are not required. Finally,
93 both modules are integrated in a courseware environment, which implements the user
94 interface and characterises the most important steps in X-ray projectional radiography.

95 Section 2 details the work related to our application. It focuses on character ani-
96 mation and X-ray simulation. Section 3 discusses the technical choices made: Using
97 a real-time animation of the anatomy and a real-time framework for the simulation of
98 X-ray images. The main features of our X-ray radiograph simulator are reviewed in
99 Section 4. Section 5 shows the final results achieved in this project. It reviews three
100 use cases (teacher's use, student's use, and exercises). A face and content validation
101 study is also provided. Section 6 provides our conclusions and discuss possible future
102 work. Finally, the appendix describes a YouTube Playlist with videos that illustrate the
103 most important functionalities of our interactive teaching and learning environment.

104 2. Related work

105 To provide the most true-to-life experience and offer a broad variety of cases, com-
106 puterised medical simulators aim to be as realistic as possible. For this purpose, virtual
107 human models are required [11]. There are commercially available anatomical virtual
108 human models, such as ZygoteBody™ [12]. An alternative is the use of real patient

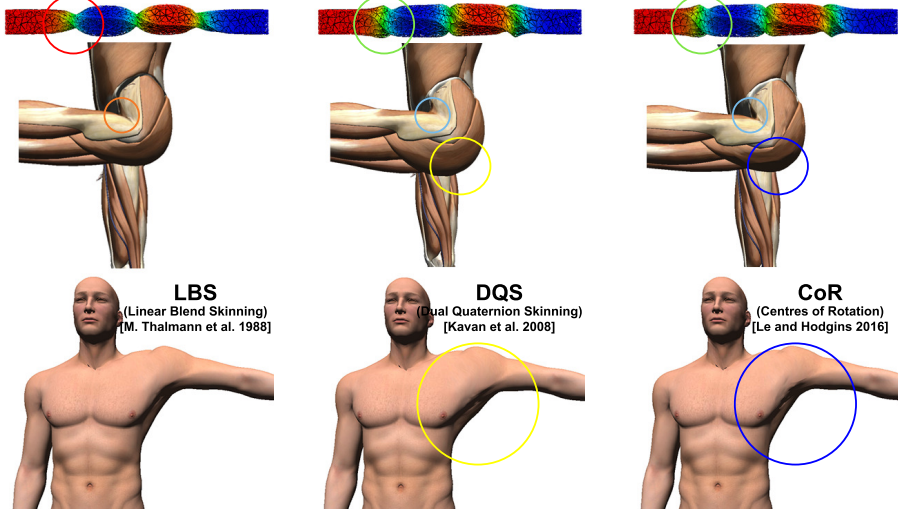
109 data captured using medical imaging techniques such as computed tomography (CT),
110 magnetic resonance imaging (MRI) and/or ultrasound (US). The rational is to provide
111 more realistic models as there are directly derived from actual patient data [13]. Al-
112 though the new generation of medical simulators have recently begun to use specific
113 patient data [14], the main problem is that those virtual patients are usually given in
114 a specific subject position. Also, the patient's position in the medical scanner may be
115 different from the one required by the simulator. Some particular procedures need the
116 patient model in a different position that it was initially recorded. The consequence is
117 that the patient data is very static and limited, and it does not represent the majority of
118 clinical cases. Character animation from CG (i.e. techniques from the film and video
119 game industries) can be used to move bones and update the skin surface accordingly.
120 However, medical simulators still need a method that deals with anatomy animation
121 including deformation of internal soft-tissues.

122 To animate virtual patient models as realistically as possible, we have considered
123 bio-mechanical and musculoskeletal techniques and physically-based models from the
124 CG literature. We can found some examples where the muscle behaviour is simulated
125 efficiently [15]. For most of these techniques, a user must perform some steps manually
126 and, in general, bio-mechanical models are not complete and localised only on a part of
127 the human anatomy [16]. Others physically-based techniques try to preserve muscle's
128 volume [17]. Muscle tissues present other problems as it is usually required to retrieve
129 the muscle's image in relaxed and extended positions. Also, there are techniques that
130 retrieve muscle-skeletal models from medical images [18].

131 All these techniques do not run at interactive rates and may require detailed infor-
132 mation of the patient which is not readily available. Often, not all patient tissues are
133 captured properly or the tissue's mechanical properties are not easy to extract from the
134 medical images. Furthermore, simulators need other anatomical structures aside from
135 simulating muscles and skeleton.

136 On the contrary, geometrically-based algorithms usually run in real-time and they
137 usually produce plausible results. Skeletal animation is the most used 3D CG technique
138 to animate articulated characters. The most widely used technique is Linear Blending
139 Skinning (LBS) [19], but it suffers well-known artefacts such as collapsing elbows
140 or candy wrapper effect which do not help to get realism in a simulator. Another
141 technique commonly used is Dual Quaternion Skinning (DQS) [20], it solves LBS's
142 problems but occasionally introduces joint-bulging artefact where meshes increase in
143 volume. Numerous alternatives to LBS and DQS can be found in the literature [21]
144 to address some of the deficiencies mentioned above, but at the cost of decreasing
145 the computational performance or leading to other artefacts. In [22], Le and Hodgins
146 solve those artefacts without needing more computational power but a high number of
147 centres of rotation must be initially calculated (see Figure 1).

148 To ease the deployment of new models by users with no or limited knowledge in
149 CG, we have focused on methods that can provide virtual patient data automatically.
150 Baran and Popović [24] proposed an automatic algorithm where they adapt a virtual
151 skeleton to any 3D model. More recent work improves this method to deal with point
152 handles, virtual bones and cages [25] (a cage defines an enclosure, using a 2D polygon
153 or a 3D polyhedron, which is used to control the deformation of an arbitrary topology).
154 It is also possible to use registration to transfer data from MRI to a desired anatomical



(a) LBS is the classic technique but suffers from candy-wrapper artefact.

(b) DQS solves candy-wrapper artefact but deformed tissues may change in volume.

(c) COR is more robust to the candy wrapper and joint-bulging artefacts [23].

Figure 1: Differences between the LBS, DQS and COR skinning techniques. The red circle depicts a candy-wrapper artefact; the orange circle depicts a collapsing elbow and the yellow circles show joint-bulging artefacts. Green circles are used when candy-wrapper artefacts are solved; cyan circles when the collapsing elbow artefact is solved and blue circles when joint-bulging artefacts are solved.

model [26]. This technique is, however, not focused on animation and does not run interactively. As an alternative, Sújar *et al* proposed a relatively similar method to deform the anatomical structures [23]. Furthermore, it is an automatic method to animate human character’s anatomy in realtime.

Another component that is required to build this interactive learning environment is the X-ray image simulator. Both accuracy and speed are requirements. Physically-based simulation frameworks exist. They are often aimed at particle physics and/or medical physics research and focus on accuracy rather than speed. These frameworks usually rely on Monte Carlo (MC) methods because they produce very realistic images [27, 28, 29]. Particles, here photons, are generated. The path of each photon through matter is tracked. At each step of the simulation, random events, such as scattering and absorption, may occur depending on probability laws that rely on the photon’s energy and the properties of the material crossed by the photon. However, MC methods are not applicable to real-time interactive applications because they have to calculate probabilistic X-ray interaction models for the transport of photons in matter and it is time consuming: To generate a relatively noise-free image, days or weeks of calculation may be needed. As a fast alternative, deterministic calculation based on ray-tracing is often used to solve the Beer-Lambert law [30, 31, 32, 33]. Freud *et al* proposed an alternative model for deterministic simulation [34]. It relies on the traditional graphics pipeline by using a modified Z-buffer algorithm [35, 36] called L-buffer. It

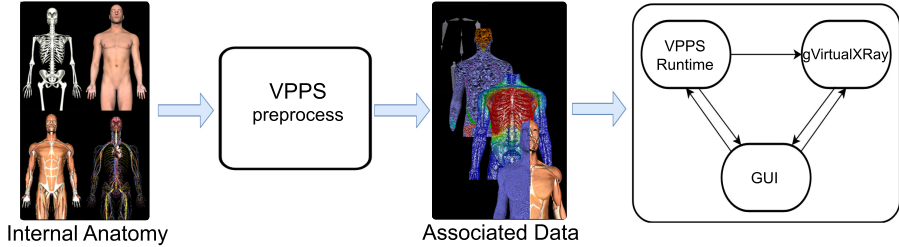


Figure 2: Simulator architecture: i) anatomical structures are preprocessed once per character, ii) then the X-Ray simulator loads the patient anatomic and the precomputed data and finally the courseware drives the training session controlling the VPPS module and gVirtualXRay. This architecture allows to run the simulation at interactive rates.

175 has been ported to the graphics processing unit (GPU) using OpenGL and its OpenGL
 176 Shading Language (GLSL) [37]. It shares the same technologies used by modern video
 177 games to provide a real-time X-ray image simulation tool. It is now available as an
 178 Open Source project, gVirtualXRay (<http://gvirtualxray.sourceforge.net/>),
 179 and can be used with various programming language such as Python, R, Ruby, GNU
 180 Octave, etc. [38]. Other GPU implementations have also been reported [39].

181 3. Simulator Components

182 We propose a tool that allows teachers and students to interact with the X-ray con-
 183 figuration and the patient’s positioning without any kind of radiological risk to the
 184 patient or even the radiographer. Our approach relies on two computationally intensive
 185 components: i) a real-time character animation framework (VPPS) that allows the
 186 virtual patient to change positions, with his/her internal anatomy being deformed ac-
 187 cordingly, and ii) an X-ray simulation library (gVirtualXRay) that generates physically-
 188 based radiographic images in realtime. Besides, the courseware module integrates both
 189 components, providing a graphical interface and simulator training functions.

190 The VPPS precomputes a significant amount of data to achieve interactive frame
 191 rates. Fortunately, all these computations can be performed only once per model. One
 192 of the most challenging requirements we face in our research was to simplify the in-
 193 corporation of new virtual patient models. Therefore, the VPPS component is split in
 194 two modules. The first one computes required pre-process data for each module and
 195 the second one adapts the patient positioning on users demand. Figure 2 summarises
 196 the overall architecture of our software.

197 3.1. Virtual Patient Positioning System

198 To let the user select a position interactively, we adapt the internal and external
 199 anatomical models of a virtual character to any desired position. We decided to follow
 200 a purely geometrical approach based on an improved skeletal animation technique [23],
 201 instead of a fully physically-based simulation algorithm, in order to meet the following
 202 requirements:

- It has to be flexible to incorporate as many existing 3D patient models as possible.
- It has to minimize the user intervention when adding new virtual patients.
- It has to run in realtime.

Skeletal animation is commonly used in the computer graphics industry to animate articulated 3D models. This type of techniques transfers the movement of a virtual skeleton to a boundary representation (B-rep) of a virtual character. The procedure is divided into three stages: rigging, weighting and skinning. The virtual skeleton, which is a hierarchical set of virtual bones, is created in the rigging phase. The weighting phase computes the influence of each virtual bone on the model vertices. Finally, the bones' movements are transferred to the vertices through a skinning technique. The main limitation of this traditional workflow is that the rigging and weighing steps are usually performed manually by a 3D artist to provide a plausible animation. Although there exist several approaches to automatise these two steps [40, 41], they are designed to work with B-reps and they cannot be used to deform internal soft-tissues.

Our method relies on a fully automatic procedure that transfers the bone movements to all tissue models. In contrast to classical skeletal animation techniques, our animation pipeline applies the bones movements to a Lagrangian mesh that discretise the interior of the virtual patient. We use the volumetric Lagrangian mesh to interpolate a displacement field, which is used to deform any available internal or external patient anatomy. In order to build the virtual skeleton and the volumetric Lagrangian mesh, the meshes corresponding to bones and the skin have to be correctly labelled and they are the only required tissues (i.e. internal tissues are optional). We have divided the animation workflow in 5 stages:

1. Rigging: We adapt a predefined virtual skeleton to the labelled bone tissue.
2. Volumetrisation: This stage automatically builds a volumetric Lagrangian mesh.
3. Weighting: Our method estimates the influence of the virtual bones on the volumetric mesh vertices, using the diffusion equation for the stationary case.
4. Mapping: Aiming at accelerating the real-time animation of the patient anatomy, all the virtual tissues are mapped into the volumetric mesh.
5. Skinning: The virtual bones movements are applied to the volumetric mesh and then transferred to the patient tissues.

The first four steps are computationally expensive and they have to be executed only once per patient. Therefore, we have grouped them in a VPPS Preprocess Module. Besides the skinning phase it can be implemented to run in modern GPUs and achieve interactive frame rates, even for complex models (see Section 5).

3.2. Virtual X-ray Imaging Library

A deterministic simulation tool is required to generate images in realtime. Monte Carlo simulation is not suitable as it cannot provide real-time performance. gVirtualXRay has been selected for the X-ray generation as it is an open-source library that makes use of portable technologies, such as the C++ language, OpenGL and GLSL for

244 the core library, and Simplified Wrapper and Interface Generator (SWIG) to generate
245 binders to other programming languages (to-date C#, Java, Octave, Perl, Python 2 and
246 Python 3, R, and Ruby are supported) [42]. gVirtualXRay also makes use of triangular
247 meshes to describe the patient’s anatomy. This requirement is shared with the real-time
248 patient positioning component. This is the most common data representation in real-
249 time 3-D graphics. Digitally reconstructed radiograph (DRR), a well-known technique
250 to generate radiographs from CT scans, has been discarded for this reason [43]. It is
251 not convenient to implement a character animation model with CT data. Also, GPU
252 handles on the triangular meshes are actually shared between the two components gVir-
253 tualXRay and the real-time patient positioning component to increase performance.

254 gVirtualXRay implements Freud *et al*’s L-buffer principle [34] on the GPU. It relies
255 on a modified rendering pipeline from 3-D computer graphics. The L-buffer aims at
256 computing the path length of X-rays through polygon meshes, from the X-ray source
257 to every pixel of the detector. It is then used to solve the Beer-Lambert law (also called
258 attenuation law) from polygon meshes. It was first implemented on GPU with a mono-
259 chromatic beam spectrum (all the photons have the same energy) and for parallel pro-
260 jections (e.g. to mimic a source far away from the scanned object as with a synchrotron)
261 and infinitesimally small point sources [37]. Extra rendering passes (i.e. loops in the
262 algorithm) were added to the rendering pipeline to allow the use of polychromatic
263 beam spectra and to model the focal spot of an X-ray tube [44]. The current version
264 of gVirtualXRay relies on the XCOM Photon Cross Sections Database from the Na-
265 tional Institute of Standards and Technology (NIST) to compute the mass attenu-
266 ation coefficient of the material of the scanned objects [45]. The material can be defined as
267 a chemical element (e.g. hydrogen), a mixture (e.g. “Ti90Al6V4” for a titanium alloy
268 with small amounts of aluminium, 6%, and vanadium, 4%), a compound (e.g. “H2O”
269 for water), or a Hounsfield unit. We chose the latter as it is commonly understood in the
270 medical community. Hounsfield units are then converted into their respective chemical
271 compositions and densities [46]. A quantitative validation study has been conducted
272 to assess the accuracy of the simulated X-ray images [38]. Geant4, a state-of-the-art
273 Monte Carlo radiation transport code by the European Organization for Nuclear Re-
274 search (CERN), is used to generate some X-ray radiographs. Each image required
275 about two weeks of computations on HPC Wales’ supercomputer. Similar radiographs
276 are simulated on the GPU with gVirtualXRay in milliseconds. Corresponding images
277 are then compared (see Figure 3 for an example). Test images produced with gVirtu-
278 alXRay are perfectly correlated with the ground-truth images produced using Geant4.

279 **4. Courseware**

280 The courseware is in charge of developing the training capabilities of the simulator,
281 integrating the previously described modules and providing a graphical user interface
282 (GUI). Figure 4 shows how the GUI looks like and the main functionalities of the
283 simulator. All the GUI widgets related to the position functionality are grouped in the
284 upper left corner of the window. In the lower left corner, the X-ray machine setup can
285 be configured. The list of patient tissues is located in the upper right corner. Finally, in
286 the lower right corner, the corresponding X-ray image is shown and it can be modified
287 using the mouse.

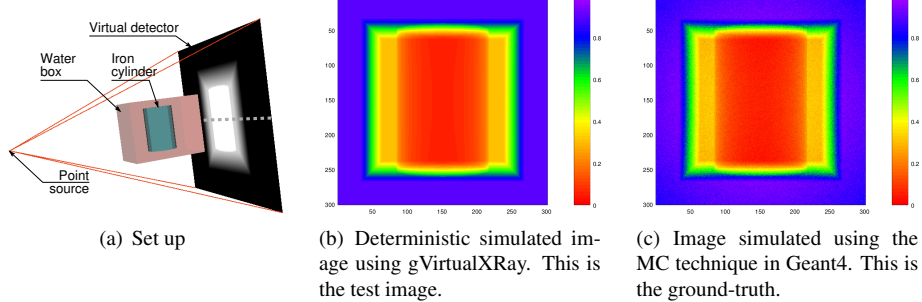


Figure 3: Example of validation test using a simple test case.



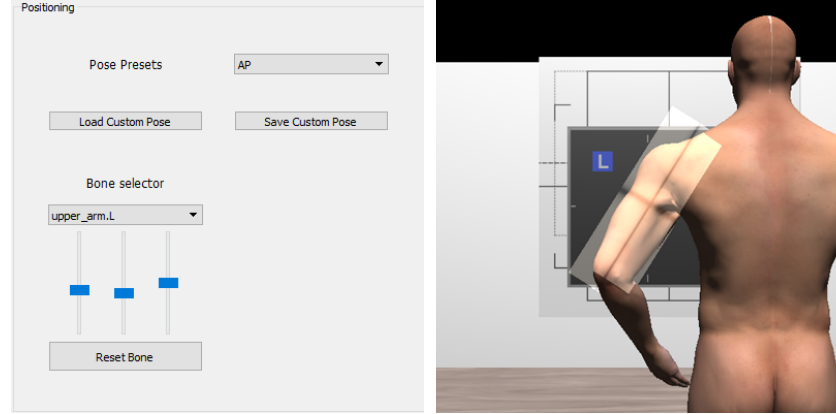
Figure 4: GUI of our projectional radiography simulator: (a) patient positioning options, (b) centring, tube voltage, source-object distance and source-cassette distance configuration (c) collimation setup, (d) tissue visibility and material properties, (e) side marker's selection and digital image manipulation.

288 This section describes its most important features. First, we explain how the pro-
289 cedure is characterised and then, the lecturing and self guided-training functionalities
290 are described.

291 *4.1. Simulation of the X-Ray procedure*

292 *4.1.1. Positioning the patient*

293 In projectional radiography, the positioning of a patient is essential in order to get
294 the best image whilst reducing the radiation dose to the minimum requirement. As
295 described in the radiographer curriculum [47], the users can choose if the patient is
296 standing up or lying down. Note that the VPPS makes use of a purely geometrical
297 algorithm and does not take into account the effect of gravity. Then, users are able to
298 define the position of a particular body part through the GUI, using a variety of methods
299 : (i) Common positions used in radiography are preset and they can be chosen from a



(a) A user defines the left arm position via the GUI.
 (b) Corresponding 3D visualisation where the virtual patient's left arm has been moved accordingly.

Figure 5: An example of virtual patient positioning.

300 top-down list; (ii) They can eventually choose any body part and move it directly. The
 301 users can then modify the position of any bone by altering the rotation angles of the
 302 corresponding joints using sliders; (iii) They can estimate the position of virtual patient
 303 using motion capture with an off-the-shelf peripheral such as the Microsoft Kinect (see
 304 <https://youtu.be/1s-eTT1pCy8> for evidence). In Figure 5, the upper arm was
 305 moved to get an lateral humerus projection. Any position can be saved so that teachers
 306 can make pre-recorded positions available to students or for future use in the classroom.
 307 Depending on the lecturer demands any of the previously described techniques can be
 308 removed from the GUI. <https://youtu.be/zitw5-Xk4dY> is a link to a video that
 309 illustrates patient positioning.

310 **4.1.2. X-ray setup**

311 Three components need to be set to simulate an X-ray image. The properties of the
 312 X-ray source, the X-ray detector (or cassette) and a virtual anatomy need to be known:

- 313 • The *X-ray source* is defined by its position, shape (e.g. parallel beam, point
 314 source, or focal spot) and beam spectrum (monochromatic or polychromatic).
 - 315 • The *X-ray detector* is defined by its position, size, resolution and orientation.
 - 316 • *Each anatomical structure* is defined by its surface as a triangular mesh and its
 317 material properties so that its linear attenuation coefficients can be computed to
 318 solve the Beer-Lambert law. We rely here on Hounsfield values and convert them
 319 into mass attenuation coefficients and densities [46].
- 320 Other parameters may also be included, e.g. collimation (see below).

321 In this medical application, whenever possible we favour parameters that are mean-
 322 ingful for the targeted community of users rather than parameters required by the sim-
 323 ulator. The user can control the relative distance between the X-ray source and the
 324 detector or cassette (known as *source to image distance (SID)* in radiography) and the
 325 distance between the X-ray source and the patient (known as *source to object distance*
 326 (*SOD*)). *Centring point* is another technical term used in radiography. [Centring is the](#)
 327 [focus point of the primary X-ray beam in relation to anatomy. This point is dictated by](#)
 328 [the anatomy that is trying to be demonstrated within an X-ray image. This point will](#)
 329 [represent the middle of the resultant X-ray.](#)

330 Centring and positioning of the patient are heavily correlated, and they actually
 331 define the relative positions of the X-ray source, of the cassette and of the patient.
 332 Therefore appropriate centring and positioning are necessary to maintain the radiation
 333 dose to its strict necessary minimum. It is assumed that a radiographer will always
 334 ensure that the centre of the body part lies at the middle of the cassette.

335 “Collimation” is another common technical term used in radiography. Lead plates
 336 or leaves can be placed at the front of the X-ray tube to limit the exposure to ionising
 337 radiation to a given area of the body. As lead is a material that heavily attenuates
 338 X-rays, hardly any radiation is deposited in the tissues protected by the collimator.
 339 Therefore appropriate collimation is also important to ensure the area of interest is
 340 definitely included on the image, limit the radiation field to that area of interest, reduce
 341 scatter in order to maintain the image quality and limit the radiation exposure of organs
 342 at risk.

343 Such important aspects of X-ray radiography can be reproduced in our virtual en-
 344 vironment. The X-ray source and cassette move as the user move the mouse in 3D
 345 visualisation window. The user can also use the GUI buttons to finely tune the pos-
 346 ition into a correct centring (see Figure 7). The X-ray beam is represented by the light
 347 projection on the patient’ skin and cassette (see Figure 6) as it is the case in the X-ray
 348 room (see Figure 15(a)).

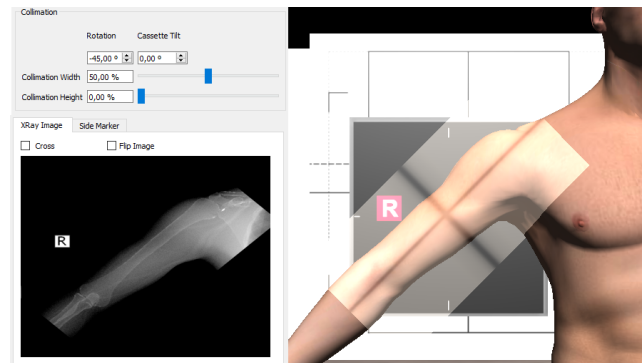


Figure 6: Collimation configuration to target the X-ray beam on the humerus only. It is rotated by 45° and the height of the beam has been reduced.

349 The X-ray beam spectrum corresponds to a tabulated list of number of photons and
 350 corresponding photon energies in kiloelectron volt (keV). In a clinical environment this

351 is controlled by radiographers via the peak kilovoltage (kVp) of the current applied to
352 the X-ray tube. Exposure factors play an important role in X-ray projectional diagnosis
353 because they can affect the quality of the produced radiograph. An inappropriate
354 exposure may decrease the contrast in X-ray images. In order to avoid mistakes and
355 avoid taking the same radiograph several times, trainees must understand how radia-
356 tion is produced by an X-ray tube and what/how parameters affect the image quality.
357 An X-ray tube contains a cathode to produce electrons and an anode, i.e. a target on
358 which the electrons will collide. If the electrons has a sufficient energy, X-rays will be
359 created. The operator can control the electrical parameters (voltage applied to the tube
360 in kilovolt (kV) and current intensity in milliampere-second (mAs)) and exposure time
361 in fraction of a second. The voltage controls the energy of the X-ray photons produced
362 by the tube. mAs controls the amount of photons produced over a set amount of time
363 (seconds). For medical diagnosis in radiography, the anode is usually made of tungsten.
364 Voltages in the 55-125 kV range are commonly used in clinical routine. Corresponding
365 spectra can be simulated using the tungsten anode spectral model using interpolating
366 polynomials (TASMIP) algorithm [48]. For each voltage in the range 30-140 kV, it
367 produces a list of photon energies in keV and relative number of photons. The user
368 can select the voltage in kV, and the corresponding beam spectrum is used to in the
369 simulation by gVirtualXRay.

370 Changing the kV value will produce different X-ray images. The X-ray radiation is
371 absorbed differently by soft than dense structures. The level of absorption varies with
372 the photon energy, but not linearly. When the kV increases, the X-ray photons can
373 penetrate more without being absorbed. On the one hand, if the kV value is too low,
374 the image will be whiter and more blurred. On the other hand, if the kV value is too
375 high, the image will be over-exposed and too dark. Our simulator can replicate such
376 behaviour (see Figure 7).

377 Note that due to the deterministic nature of the X-ray simulation algorithm, mAs
378 cannot be directly taken into account. However it is possible to mimic a low mAs value
379 by adding Poisson noise to the simulated X-ray image.

380 4.1.3. *Cassette's side markers*

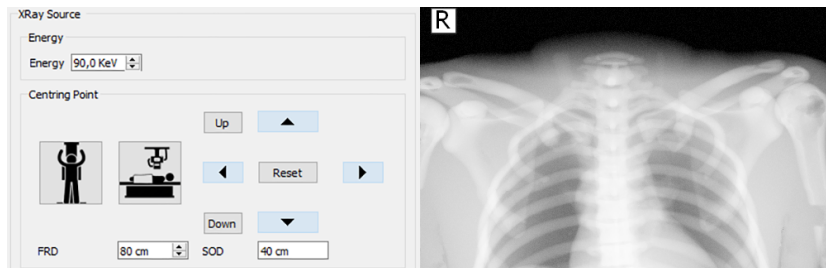
381 In clinical radiography, an anatomical marker is placed within the field of the X-
382 ray source, and clear of the area of interest. It aims to identify the left- and right-hand
383 sides of the patient. This is because the left-hand side of the patient may not be on
384 the left of the image. This practice is mandatory to avoid misinterpretation of the
385 X-ray image. In our tool, a 2D widget allows to interactively place a side marker
386 over the cassette using the mouse. This 2D widget transfers this 2D position on the
387 cassette to the 3D visualisation of the cassette in the virtual environment. Additionally,
388 this side marker appears on the X-ray image and can be saved in an image file. See
389 <https://youtu.be/EDJM3pSWtgo> for an illustrative video. Figure 8 shows the side
390 markers in the 3D visualisation and in the corresponding X-ray image.

391 4.1.4. *Digital image manipulation*

392 Nowadays, digital X-ray detectors are used in modern hospitals rather than tradi-
393 tional X-ray film. The X-ray image is captured directly to a bitmap by the detector, and
394 it is possible to display it using a computer. The greatest advantage of digital imaging



(a) X-ray image simulated using a 60 kVp X-ray tube voltage. The incident energy produced by the X-ray tube is too low to sufficiently penetrate the tissues and differentiate them on the X-ray image.



(b) X-ray image simulated using 90 kVp X-ray tube voltage. The contrast between tissues has improved.

Figure 7: Effect of the X-ray tube voltage on an X-ray image of the chest.

395 is the ability to duplicate, store and manipulate the data. For example, image filtering
 396 can be used to reduce minor problems due to overexposure or underexposure, and
 397 perform some measurements (e.g. compute the distance between two different anatomical
 398 landmarks). Digital images can also be used in computer-aided diagnostic (CAD)
 399 software. Our user interface provides a few simple image processing filters that allow
 400 users to enhance resulting images (e.g. to get a better interpretation of the anatomical
 401 tissues). A Log-Scale filter and a Gamma filter can be selected to improve the final
 402 image. The brightness and contrast can also be altered to emphasise each tissue or
 403 highlight a particular zone. In medical applications, X-ray images are often shown in
 404 *negative*, so that bones are in white and air in black. All these filters can be easily used
 405 by clicking with the mouse over the X-ray image. Figure 9 shows examples of image
 406 manipulation applied on the same X-ray image. In Figure 9(a), coins can easily be seen
 407 on the image compared to Figures 9(b) and 9(c). Also, the anatomical side marker is
 408 present to determine the anatomical side of body on the radiographic image. Finally,
 409 users can save any X-ray radiograph they want to in an image file on the hard drive.
 410 See <https://youtu.be/x7KGsNSMSh8> for a video that focuses on the digital image
 411 manipulation.

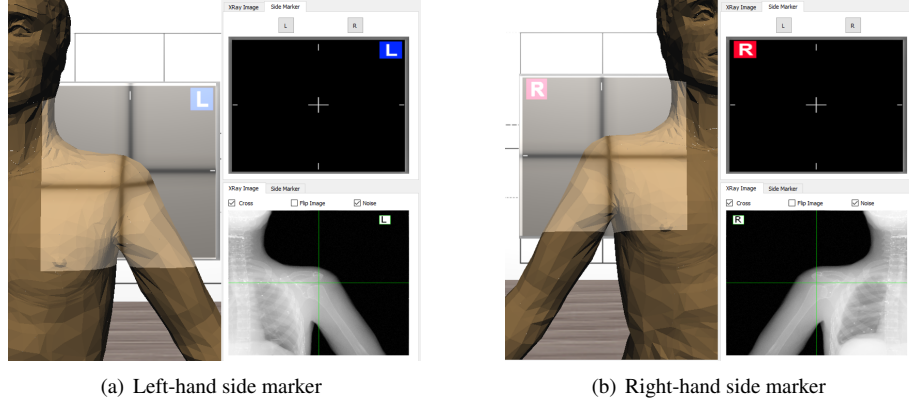


Figure 8: The user can select between the left and right side markers and place it over the cassette.

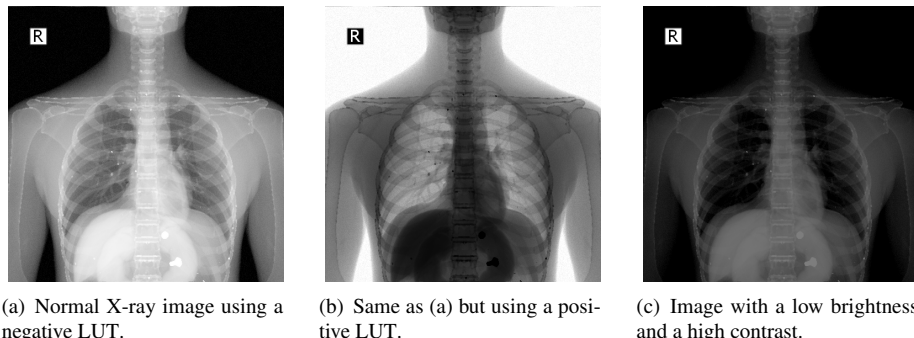
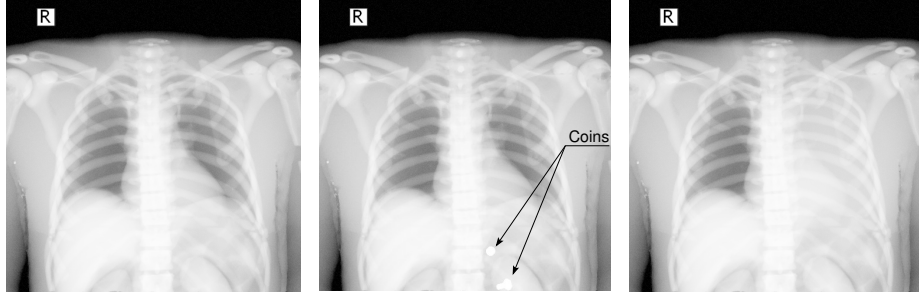


Figure 9: Our tool allows digital image manipulation.

412 4.2. Lecturing features

413 Our simulator provides additional features which will support the instructor in the
 414 classroom environment, although they are not directly related to the simulation of any
 415 step of the diagnostic radiography procedure. The system allows to show and hide
 416 specific tissues of the virtual patient at run time. For example, the user can modify the
 417 opacity of the skin surface to reveal internal structures in the 3D visualisation. This
 418 way students can understand the relationship between the different body tissues and
 419 X-ray images.

420 It is also possible to modify the tissues properties with respect to X-ray attenuation
 421 using the Hounsfield Scale. Hounsfield values can be converted into list of chemical
 422 elements, etc. [46] so that corresponding linear attenuation coefficients can be com-
 423 puted from photon cross-sections [45] to solve the Beer-Lambert law for any incident
 424 energy. Being able to change the tissues properties allows teachers to show a variety
 425 of diseases, e.g. a calcified bone, a collapsed lung (see Figure 10(c)), or an air-filled
 426 stomach. It is even possible to introduce foreign objects inside the internal anatomy.



(a) Normal AP Chest X-ray image
 (b) Same image as (a) but with foreign objects in the stomach.
 (c) Same image as (a) but with a collapsed lung.

Figure 10: The X-Ray attenuation properties of the tissues can be modified to simulate different scenarios.

427 For example, Figures 9 and 10(b) show coins in the stomach. See the following video
 428 for further details: <https://youtu.be/02K2ojcExTc>.

429 *4.3. Self-guided training*

430 Performing diagnostic radiography requires both theoretical and non-cognitive skills.
 431 The only effective way of acquiring non-cognitive skills is practice. It is now well es-
 432 tablished that VR resources and computerised simulators can be exploited to guide and
 433 boost the trainees' learning process. Interactive tools can also be designed to promote
 434 self-directed learning. With this regard, our simulator provides a guided mode that
 435 leads users along the procedure. This mode explains the X-ray projection procedure
 436 step-by-step and offers additional information if the user requires it. Finally, the system
 437 evaluates the user's performance and retrieves assessment metrics. Besides, we offer set
 438 of non-guided exercises that allows the instructor to check the evolution of the trainees.
 439 Finally, we have created a set of videos to help the users to get used to the simulator.
 440 See the following videos for further information: <https://youtu.be/EdyDqvGr8ww>
 441 and <https://youtu.be/WFOAVSLXufs>.

442 **5. Results**

443 The proposed X-Ray simulator offers a teaching and learning platform where third
 444 party anatomic models can be easily integrated. To test the viability of our approach,
 445 we incorporated the following models:

- 446 • ZygoteBody™ 3D Poly Models [12]. This set of virtual patient models provide
 447 B-Reps of the most important tissues. We used female (ZF) and male (ZM)
 448 models.
- 449 • Anatomium™ 3D Human Anatomy Digital Data Sets [49] offer several virtual
 450 patients. Similarly to ZygoteBody, they include the B-reps of several tissues.
 451 We used one of the available male models.

Table 1: Model complexity.

Model	Superficial Mesh		Volumetric Mesh	
	Vertices	Triangles	Nodes	Tetrahedrons
<u>ZygoteBody</u> TM Male [53]	1317862	2601469	553412	2576779
<u>ZygoteBody</u> TM Female [53]	1468989	2896011	492646	2314456
Anatomium Male [49]	790461	1570778	767325	3411170
<u>Segmented Inner Organs</u> [51]	591265	1184325	242033	1182485

- 452 • Voxel-Man’s Segmented Inner Organs [50, 51]. This model is composed by a
 453 set of segmented volumetric images obtained from the Visible Human data set.
 454 To incorporate this model, we generate surface meshes using the marching cubes
 455 algorithm [52].

456 Figure 11 depicts the visual results obtained for these models and Table 1 shows the
 457 complexity of each model. As it was expected, the quality of the final image depends
 458 to a large extend on the quality of the virtual patient model. We found that some gen-
 459 eral purpose models need further preprocessing to obtain plausible images. Bones are
 460 made of two types of tissues. The outer layer of bones is called cortical bones. They are
 461 strong and dense. The inner layer, called trabecular bone, is a lot less dense. Comercial
 462 3D virtual models often only provide the bone structures as the surface of the cortical
 463 bones. Trabecular bone are almost systematically ignored. Other types of tissues are
 464 also provided as their superficial representation, i.e. without nothing inside. However,
 465 gVirtualXRay works as a ray tracer where a ray goes through an anatomical structure
 466 (front face of a triangle) and get out of the same structure (back face of a triangle) in or-
 467 der to calculate the light attenuation depending on the material properties associated to
 468 this anatomical structure and the length of ray crossing it. This solution does not work
 469 particularly well with bones because their internal layers attenuate X-rays a lot less.
 470 As a consequence, if no particular care is given to bones, they will have an homoge-
 471 neous look in the simulated X-ray images, which is not very realistic (see Figure 12(a)).
 472 To solve this deficiency, we added a new mesh for each bone to depict the trabecular
 473 bones. It can be efficiently achieved by duplicating the surface mesh of the cortical
 474 bones, shrinking them a little bit, and inverting their normal vectors. Figure 12 depicts
 475 the difference between the original meshes without trabecular bones and the modified
 476 meshes with trabecular bones. Note that this issue does not occur when working with
 477 surface meshes extracted from segmented CT dataset as cortical and trabecular bones
 478 are easy to identify and separate in CT data. Regarding the patient positioning, the
 479 VPPS module worked seamlessly with all the models used in the evaluation.

480 VR simulators required interactive frame rates to guaranty an adequate user expe-
 481 rience. For this reason, VPPS and gVirtualXRay were implemented to run efficiently
 482 in modern GPUs. Besides, both modules share GPU memory to reduce the data trans-
 483 ferred through the system busses. The performance was tested on an Intel®i7-3770 @

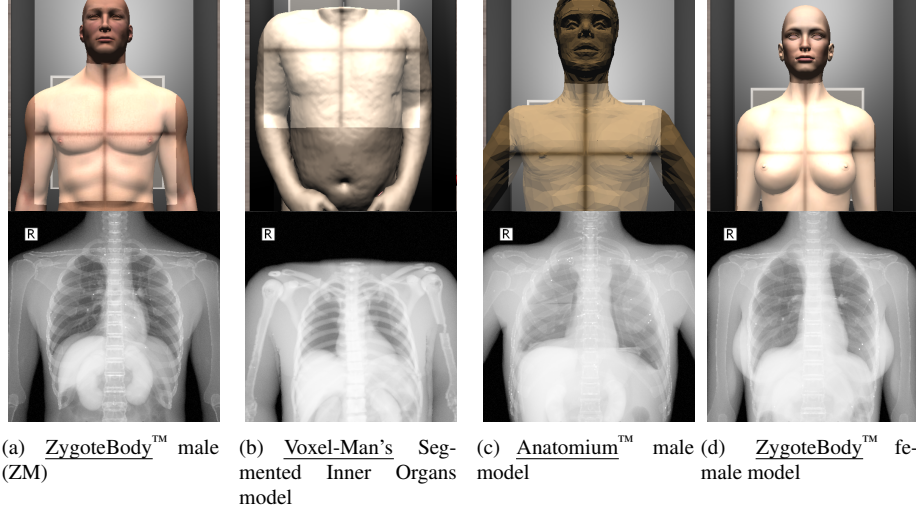


Figure 11: Results obtained using different anatomical models.

484 3.7GHz CPU with 16GB of Random Access Memory (RAM) and a NVIDIA® Quadro
485 K5000 graphics card with 4GB of graphics memory. In the worse case (ZM), the frame
486 rate is over 30 fps. However, the preprocessing module requires about 7 minutes for
487 each virtual patient.

488 Regarding the evaluation of the training capabilities of our simulations, we have
489 designed a test that can be found in <https://goo.gl/forms/cghkCHtylUt8ixzw1>.
490 18 participants run the experiment, 16 experts in the procedure and XXX xxx-year
491 students.

492 For face validity, 14 questions related to the realism of the simulator and its func-
493 tionality, as given in Table 2.

494 Figure 13 shows the results of these questions for all participants.

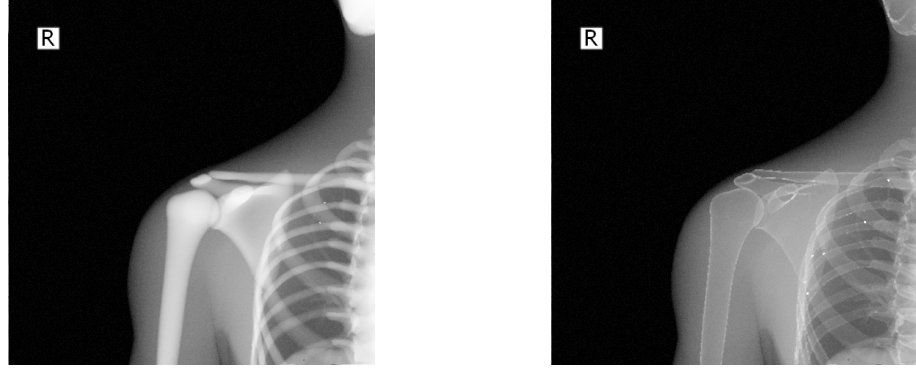
495 For content validity, 11 questions related to the main purpose of the simulator and
496 the courseware, as given in Table 3.

497 Figure 14 shows the results of these questions for all participants.

498 6. Conclusions

499 In this paper, we presented a VR teaching and learning environment for diagnostic
500 radiography. It relies on i) an interactive character animation method for the patient
501 positioning and deformation of internal tissues, and ii) a real-time X-ray simulation
502 library. We developed a courseware module that turns our tool into a training sys-
503 tem. It is now well established that VR resources and computerised simulators can
504 be exploited to guide and boost the trainees' learning process. Radiographers have to
505 know both how to position a patient and how to tune an X-ray tube to avoid clinically
506 unnecessary radiation doses and repetitive acquisitions of X-ray images. Our system
507 provides a safe environment where the procedure can be rehearsed, reducing all kinds

To be com-
pleted once
we have
the feed-
back from
GRAHAM
and his
colleagues
(question-
naires)



(a) Original ZygoteBody™ model without soft and hard bone differentiation.

(b) Same model as (a) but with added internal structures.

Figure 12: Solving the absence of internal structures in bone.

of radiological risk to the patient or even the radiographer. It is important to highlight that the proposed system does not substitute traditional teaching methods but enhance the learning process overcoming their main limitations. Figure 15 compares a specific projection from a text book [47] with a simulation of the same projection. The real and the virtual patient used to generate both images are also shown. Both, real patient data bases and text books are the preferred approaches to get theoretical skills, while our simulator allows to interactively perform the main steps of the procedure in order to train non-cognitive skills.

We have designed the courseware module to include functionalities to assist the teacher during the lecture and for self-directed leaning. Allowing repetitions without any radiation risk, it is useful in both environments. Since, the positioning tool and the X-ray image simulation achieve interactive frame rates, the teachers and students can select the anatomy position and the machine set-up and see the corresponding changes in X-ray image in realtime. In the classroom, teachers can discuss a given procedure, e.g. what is important and the pitfalls to avoid. They can interactively show a good picture (good positioning, centring, collimation, and setting of the X-ray machine) and bad ones. In contrast, the courseware guides the students through the procedure and they can see the actual consequences of their mistakes. Additionally, we provide a non-guided mode, where the system asks the student for an specific projection (see Figure 16)

Our solution was designed to facilitate the incorporation of new virtual patient models. Section 5 shows how several third party models were successfully integrated. This functionality was particularly challenging since our tool allows the user to modify interactively the patient’s position and very few constraints are imposed to the models. Indeed, only the skin and bone tissues of the virtual patient need to be properly labelled. Currently, the scientific community is putting a lot of effort in developing new techniques for creating virtual patient to be used in VR medical trainers and planners[54, 55]. The proposed X-Ray simulator will benefit from these interest as

536 most of these techniques are compatible with our approach. On the same way, other
537 medical imaging process can be simulated and integrated in the same tool. Recently,
538 there are projects trying to simulate effectively techniques like MRI or CT which re-
539 quires some patient position knowledge.

540 In this paper we have conducted a set of experiments to probe face and content
541 validation. However, further tests will be need the to proof whether the simulator is
542 helpful for apprentices to get the curriculum of the Radiographer faster and better than
543 only depending on the teaching files.

544 The positioning system sacrifices accuracy in favour of computational performance
545 and flexibility. Natural phenomena such as gravity cannot be simulated. As a result
546 of using a geometrically-based algorithm, its plausible positions are only oriented for
547 training and educational purposes.

548 Nevertheless, this tool has some limitations about the full procedure of imaging
549 diagnostic. There are important concerns like the patient preparation which is not
550 covered in this tool:

- 551 • Physician must employ appropriate and effective communication with patients
- 552 • Patient is indicated about remove clothes or artefacts over the relevant examina-
553 tion area.
- 554 • Recommendations about use lead rubber either on patients or radiographers.
- 555 • Some assessments which involve medical conditions or protocols like pregnancy,
556 correct patient identification, etc...

557 Finally, we would like to remark that computerised systems are very good regis-
558 tering the user actions. All this information can be used to develop a set of assess-
559 ment metric that will serve to provide the trainees with information to boost their self-
560 learning processes and to evaluate their proficiency. The definition of a valid set of
561 assessment metrics will be explored in our future work.

562 Acknowledgements

563 The research leading to these results has been partially funding by the follow-
564 ing entities: the Spanish Government [Cajal Blue Brain Project, Spanish partner
565 of the Blue Brain Project initiative from EPFL; and grants TIN2014-57481-C2-1-R,
566 TIN2017-83132-C2-1-R and FPU15/05747] and European Commission [under grant
567 agreements: HBP - Human Brain Project - FET Flagship HBP604102; RaSimAS: Re-
568 gional Anaesthesia Simulator and Assistant - FP7-ICT 610425, and Fly4PET: Fly Al-
569 gorithm in PET Reconstruction for Radiotherapy Treatment Planning - FP7-PEOPLE-
570 2012-CIG 321968].

571 Some examples were based on the Visible Human male data set (National Library
572 of Medicine) and the Segmented Inner Organs (Voxel-Man).

573 We would like to thanks HPC Wales for the use of its supercomputer during the
574 validation of gVirtualXRay and NVIDIA for donating the GPU that was used during
575 the implementation of gVirtualXRay.

Check at
the end,
once we
have the
feedback
from GRA-
HAM and
his col-
leagues
(question-
naires)

576 **Acronyms**

577 **B-rep** boundary representation.

578 **CAD** computer-aided diagnostic.

579 **CERN** European Organization for Nuclear Research.

580 **CG** computer graphics.

581 **COR** Centre of Rotation.

582 **CT** computed tomography.

583 **DQS** Dual Quaternion Skinning.

584 **DRR** digitally reconstructed radiograph.

585 **GLSL** OpenGL Shading Language.

586 **GPU** graphics processing unit.

587 **GUI** graphical user interface.

588 **keV** kiloelectron volt.

589 **kV** kilovolt.

590 **kVp** peak kilovoltage.

591 **LBS** Linear Blending Skinning.

592 **LUT** lookup table.

593 **mAs** milliampere-second.

594 **MC** Monte Carlo.

595 **MRI** magnetic resonance imaging.

596 **NIST** National Institute of Standards and Technology.

597 **RAM** Random Access Memory.

598 **SID** source to image distance.

599 **SOD** source to object distance.

600 **SWIG** Simplified Wrapper and Interface Generator.

601 **TASMIP** tungsten anode spectral model using interpolating polynomials.

602 **US** ultrasound.

603 **VPPS** Virtual Patient Positioning System.

604 **VR** Virtual reality.

605 **References**

- 606 [1] P. Deshpande, A. Rasin, E. Brown, J. Furst, D. Raicu, S. Montner, S. Armato III,
607 An integrated database and smart search tool for medical knowledge extraction
608 from radiology teaching files, in: Proceedings of Workshop on Medical Informat-
609 ics and Healthcare, 2017, pp. 10–18.
- 610 [2] R. Spouge, Review of UBC Radiology Teaching App, *Journal of Digital Imaging*
611 doi:10.1007/s10278-017-0034-y.
- 612 [3] A. Bernardo, Virtual reality and simulation in neurosurgical training, *World Neu-
613 rosurgery* 106 (2017) 1015–1029. doi:10.1016/j.wneu.2017.06.140.
- 614 [4] G. S. Ruthenbeck, K. J. Reynolds, Virtual reality for medical training: the state-
615 of-the-art, *Journal of Simulation* 9 (1) (2015) 16–26. doi:10.1057/jos.2014.
616 14.
- 617 [5] J. Cecil, A. Gupta, M. Pirela-Cruz, An advanced simulator for orthopedic surgical
618 training, *International journal of computer assisted radiology and surgery* 13 (2)
619 (2018) 305–319. doi:10.1007/s11548-017-1688-0.
- 620 [6] P. Korzeniowski, R. J. White, F. Bello, VCSim3: a VR simulator for cardiovascular
621 interventions, *International journal of computer assisted radiology and surgery*
622 13 (1) (2018) 135–149. doi:10.1007/s11548-017-1679-1.
- 623 [7] R. Patel, R. Dennick, Simulation based teaching in interventional radiology train-
624 ing: is it effective?, *Clinical Radiology* 72 (3) (2017) 266.e7–266.e14. doi:
625 10.1016/j.crad.2016.10.014.
- 626 [8] P.-F. Villard, F. P. Vidal, L. Ap Cenydd, R. Holbrey, S. Pisharody, S. Johnson,
627 A. Bulpitt, N. W. John, F. Bello, D. Gould, Interventional radiology virtual sim-
628 ulator for liver biopsy, *International journal of computer assisted radiology and*
629 *surgery* 9 (2) (2014) 255–267. doi:10.1007/s11548-013-0929-0.
- 630 [9] M. Shanahan, Student perspective on using a virtual radiography simulation, *Ra-
631 diography* 22 (3) (2016) 217–222. doi:10.1016/j.radi.2016.02.004.
- 632 [10] P. Bridge, T. Gunn, L. Kastanis, D. Pack, P. Rowntree, D. Starkey, G. Mahoney,
633 C. Berry, V. Braithwaite, K. Wilson-Stewart, The development and evaluation of
634 a medical imaging training immersive environment, *Journal of Medical Radiation*
635 *Sciences* 61 (3) (2014) 159–165. doi:10.1002/jmrs.60.

- 636 [11] B. Preim, P. Saalfeld, A survey of virtual human anatomy education systems,
637 Computers & Graphics 71 (2018) 132–153. doi:10.1016/j.cag.2018.01.
638 005.
- 639 [12] Zygote Media Group, ZygoteBody, <https://www.zygotebody.com/>, ac-
640 cessed: 2018-11-08 (2018).
- 641 [13] J. E. de Oliveira, P. Giessler, A. Keszei, A. Herrler, T. M. Deserno, Surface mesh
642 to voxel data registration for patient-specific anatomical modeling, in: Medical
643 Imaging 2016: Image-Guided Procedures, Robotic Interventions, and Modeling,
644 Vol. 9786, International Society for Optics and Photonics, 2016, p. 978625. doi:
645 10.1117/12.2217491.
- 646 [14] J. Zhang, J. Chang, X. Yang, J. J. Zhang, Virtual reality surgery simulation: A
647 survey on patient specific solution, in: J. Chang, J. J. Zhang, N. Magnenat Thal-
648 mann, S.-M. Hu, R. Tong, W. Wang (Eds.), Next Generation Computer Anima-
649 tion Techniques, Vol. 10582 of Lecture Notes in Computer Science, Springer In-
650 ternational Publishing, Cham, 2017, pp. 220–233. doi:10.1007/978-3-319-
651 69487-0_16.
- 652 [15] A. Rajagopal, C. L. Dembia, M. S. DeMers, D. D. Delp, J. L. Hicks, S. L. Delp,
653 Full-body musculoskeletal model for muscle-driven simulation of human gait,
654 IEEE Transactions on Biomedical Engineering 63 (10) (2016) 2068–2079. doi:
655 10.1109/TBME.2016.2586891.
- 656 [16] A.-E. Ichim, P. Kadlecák, L. Kavan, M. Pauly, Phace: Physics-based face mod-
657eling and animation, ACM Trans. Graph. 36 (4) (2017) 153:1–153:14. doi:
658 10.1145/3072959.3073664.
- 659 [17] Y. Fan, J. Litven, D. K. Pai, Active volumetric musculoskeletal systems, ACM
660 Trans. Graph. 33 (4) (2014) 152:1–152:9. doi:10.1145/2601097.2601215.
- 661 [18] T. T. Dao, P. Pouletaut, F. Charleux, Á. Lazáry, P. Eltes, P. P. Varga, M. C. H. B.
662 Tho, Multimodal medical imaging (CT and dynamic MRI) data and computer-
663 graphics multi-physical model for the estimation of patient specific lumbar spine
664 muscle forces, Data & Knowledge Engineering 96-97 (2015) 3–18. doi:10.
665 1016/j.datak.2015.04.001.
- 666 [19] N. Magnenat-Thalmann, R. Laperrière, D. Thalmann, Joint-dependent local de-
667 formations for hand animation and object grasping, in: Proceedings on Graphics
668 Interface '88, Canadian Information Processing Society, Toronto, Ont., Canada,
669 Canada, 1988, pp. 26–33.
670 URL <http://dl.acm.org/citation.cfm?id=102313.102317>
- 671 [20] L. Kavan, S. Collins, J. Žára, C. O'Sullivan, Skinning with dual quaternions, in:
672 Proceedings of the 2007 Symposium on Interactive 3D Graphics and Games, I3D
673 '07, ACM, New York, NY, USA, 2007, pp. 39–46. doi:10.1145/1230100.
674 1230107.

- 675 [21] N. A. Rumman, M. Fratarcangeli, State of the art in skinning techniques for ar-
 676 ticulated deformable characters, in: Proceedings of the 11th Joint Conference
 677 on Computer Vision, Imaging and Computer Graphics Theory and Applications:
 678 Volume 1: GRAPP, SCITEPRESS-Science and Technology Publications, Lda,
 679 2016, pp. 200–212.
- 680 [22] B. H. Le, J. K. Hodgins, Real-time skeletal skinning with optimized centers of ro-
 681 tation, ACM Trans. Graph. 35 (4) (2016) 37:1–37:10. doi:10.1145/2897824.
 682 2925959.
- 683 [23] A. Sújar, J. J. Casafranca, A. Serrurier, M. García, Real-time animation of human
 684 characters' anatomy, Computers & Graphics 74 (2018) 268–277. doi:10.1016/
 685 j.cag.2018.05.025.
- 686 [24] I. Baran, J. Popović, Automatic rigging and animation of 3D characters, ACM
 687 Trans. Graph. 26 (3) (2007) 72:1–72:8. doi:10.1145/1276377.1276467.
- 688 [25] A. Jacobson, I. Baran, J. Popović, O. Sorkine-Hornung, Bounded biharmonic
 689 weights for real-time deformation, Commun. ACM 57 (4) (2014) 99–106. doi:
 690 10.1145/2578850.
- 691 [26] A.-H. Dicko, T. Liu, B. Gilles, L. Kavan, F. Faure, O. Palombi, M.-P. Cani,
 692 Anatomy transfer, ACM Trans. Graph. 32 (6) (2013) 188:1–188:8. doi:10.
 693 1145/2508363.2508415.
- 694 [27] S. Agostinelli, et al., Geant4—a simulation toolkit, Nucl Instrum Methods Phys
 695 Res A 506 (3) (2003) 250–303. doi:10.1016/S0168-9002(03)01368-8.
- 696 [28] A. Bielajew, et al., History, overview and recent improvements of EGS4,
 697 Tech. rep., Stanford Linear Accelerator Center (SLAC) (2004). doi:10.2172/
 698 839781.
- 699 [29] J. Baró, J. Sempau, J. M. Fernández-Varea, F. Salvat, PENELOPE: An algorithm
 700 for Monte Carlo simulation of the penetration and energy loss of electrons and
 701 positrons in matter, Nucl Instrum Methods Phys Res B 100 (1) (1995) 31–46.
 702 doi:10.1016/0168-583X(95)00349-5.
- 703 [30] F. Inanc, J. N. Gray, T. Jensen, J. Xu, Human body radiography simulations: de-
 704 velopment of a virtual radiography environment, in: Proc.SPIE, Vol. 3336, 1998,
 705 p. 8. doi:10.1117/12.317091.
- 706 [31] A. Glière, Sindbad: From CAD model to synthetic radiographs, in: Review of
 707 Progress in Quantitative Nondestructive Evaluation: Volume 17A, Springer US,
 708 Boston, MA, 1998, pp. 387–394. doi:10.1007/978-1-4615-5339-7_49.
- 709 [32] G.-R. Tillack, C. Bellon, C. Nockemann, Computer simulation of radiographic
 710 process - a study of complex component and defect geometry, in: Review of
 711 Progress in Quantitative Nondestructive Evaluation: Volume 14, Springer US,
 712 Boston, MA, 1995, pp. 665–672. doi:10.1007/978-1-4615-1987-4_82.

- 713 [33] D. Lazos, Z. Kolisti, N. Pallikarakis, A software data generator for radio-
 714 graphic imaging investigations, *IEEE Transactions on Information Technology*
 715 in Biomedicine
- 4 (1) (2000) 76–79. doi:10.1109/4233.826863.
- 716 [34] N. Freud, P. Duvauchelle, J. M. Létang, D. Babot, Fast and robust ray casting
 717 algorithms for virtual X-ray imaging, *Nucl Instrum Methods Phys Res B* 248 (1)
 718 (2006) 175–180. doi:10.1016/j.nimb.2006.03.009.
- 719 [35] W. Straßer, Schnelle kurven- und flächendarstellung auf graphischen sichtgeräten,
 720 Ph.D. thesis, TU Berlin (1974).
- 721 [36] E. E. Catmull, A subdivision algorithm for computer display of curved surfaces,
 722 Ph.D. thesis, The University of Utah (1974).
- 723 [37] F. P. Vidal, M. Garnier, N. Freud, J. M. Létang, N. W. John, Simulation of X-ray
 724 Attenuation on the GPU, in: W. Tang, J. Collomosse (Eds.), *Theory and Practice*
 725 of Computer Graphics, The Eurographics Association, 2009, pp. 25–32. doi:
 726 10.2312/LocalChapterEvents/TPCG/TPCG09/025–032.
- 727 [38] F. P. Vidal, P.-F. Villard, Development and validation of real-time simulation of x-
 728 ray imaging with respiratory motion, *Computerized Medical Imaging and Graph-*
 729 *ics* 49 (2016) 1–15. doi:10.1016/j.compmedimag.2015.12.002.
- 730 [39] Q. Gong, R.-I. Stoian, D. S. Coccarelli, J. A. Greenberg, E. Vera, M. E. Gehm,
 731 Rapid simulation of x-ray transmission imaging for baggage inspection via gpu-
 732 based ray-tracing, *Nuclear Instruments and Methods in Physics Research Section*
 733 *B: Beam Interactions with Materials and Atoms* 415 (2018) 100–109. doi:10.
 734 1016/j.nimb.2017.09.035.
- 735 [40] P. Borosán, M. Jin, D. DeCarlo, Y. Gingold, A. Nealen, RigMesh: Automatic rig-
 736 ging for part-based shape modeling and deformation, *ACM Trans. Graph.* 31 (6)
 737 (2012) 198:1–198:9. doi:10.1145/2366145.2366217.
- 738 [41] C.-H. Huang, E. Boyer, S. Ilic, Robust human body shape and pose tracking, in:
 739 *Proceedings of the 2013 International Conference on 3D Vision, 3DV ’13*, IEEE
 740 Computer Society, Washington, DC, USA, 2013, pp. 287–294. doi:10.1109/
 741 3DV.2013.45.
- 742 [42] D. M. Beazley, SWIG: An easy to use tool for integrating scripting languages
 743 with C and C++, in: *Proceedings of the 4th Conference on USENIX Tcl/Tk*
 744 *Workshop*, 1996 - Volume 4, *TCLTK’96*, USENIX Association, Berkeley, CA,
 745 USA, 1996, pp. 15–15.
 746 URL <http://dl.acm.org/citation.cfm?id=1267498.1267513>
- 747 [43] J. M. Galvin, C. Sims, G. Dominiak, J. S. Cooper, The use of digitally recon-
 748 structed radiographs for three-dimensional treatment planning and ct-simulation,
 749 *International Journal of Radiation Oncology*Biology*Physics* 31 (4) (1995)
 750 935–942. doi:10.1016/0360-3016(94)00503-6.

- 751 [44] F. P. Vidal, M. Garnier, N. Freud, J. M. Létang, N. W. John, Accelerated deterministic simulation of x-ray attenuation using graphics hardware, in: Eurographics 752 2010 - Poster, Eurographics Association, Norrk”oping, Sweden, 2010, p. Poster 753 5011.
- 754
- 755 [45] M. J. Berger, J. H. Hubbell, S. M. Seltzer, J. Chang, J. S. Coursey, R. Sukumar, 756 D. S. Zucker, K. Olsen, XCOM: Photon cross section database, Tech. Rep. NB- 757 SIR 87-3597, National Institute of Standards and Technology, Gaithersburg, MD 758 (2010). doi:10.18434/T48G6X.
759 URL <http://physics.nist.gov/xcom>
- 760 [46] W. Schneider, T. Bortfeld, W. Schlegel, Correlation between CT numbers and tissue 761 parameters needed for Monte Carlo simulations of clinical dose distributions, 762 Physics in Medicine & Biology 45 (2) (2000) 459–478. doi:10.1088/0031- 763 9155/45/2/314.
- 764 [47] E. Carver, B. Carver, Medical Imaging: Techniques, Reflection & Evaluation, 765 2nd Edition, Elsevier Health Sciences, 2012.
- 766 [48] J. M. Boone, J. A. Seibert, An accurate method for computer-generating tungsten 767 anode X-ray spectra from 30 to 140 kV, Medical Physics 24 (11) (1997) 1661– 768 1670. doi:10.1118/1.597953.
- 769 [49] 21st Century Solutions Ltd, Digital human 3D body anatomy, <http://www.anatomium.com/>, accessed: 2018-11-08.
- 770
- 771 [50] U. Tiede, A. Pommert, B. Pflessner, E. Richter, M. Riemer, T. Schiemann, R. Schu- 772 bert, U. Schumacher, K. H. Höhne, A high-resolution model of the inner organs 773 based on the visible muman data set, Journal of Visualization 5 (3) (2002) 212– 774 212. doi:10.1007/BF03182328.
- 775 [51] Segmented Inner Organs (SIO) Group, Voxel-Man, [https://www.voxel- 777 man.com/segmented-inner-organs-of-the-visible-human/](https://www.voxel- 776 man.com/segmented-inner-organs-of-the-visible-human/), accessed: 2018-11-08.
- 778 [52] W. E. Lorensen, H. E. Cline, Marching cubes: A high resolution 3D surface 779 construction algorithm, SIGGRAPH Comput. Graph. 21 (4) (1987) 163–169. 780 doi:10.1145/37402.37422.
- 781 [53] R. Kelc, Zygote body: A new interactive 3-dimensional didactical tool for teach- 782 ing anatomy, WebmedCentral ANATOMY 3 (1). doi:10.9754/journal.wmc. 783 2012.002903.
- 784 [54] W. I. M. Willaert, R. Aggarwal, I. Van Herzele, N. J. Cheshire, F. E. Ver- 785 massen, Recent advancements in medical simulation: patient-specific virtual 786 reality simulation, World journal of surgery 36 (7) (2012) 1703–1712. doi: 787 10.1007/s00268-012-1489-0.

788 [55] E. Votta, T. B. Le, M. Stevanella, L. Fusini, E. G. Caiani, A. Redaelli,
789 F. Sotiropoulos, Toward patient-specific simulations of cardiac valves: state-of-
790 the-art and future directions, Journal of biomechanics 46 (2) (2013) 217–228.
791 doi:10.1016/j.jbiomech.2012.10.026.

792 **Appendix A. YouTube playlist**

793 We provide a YouTube playlist for the reader’s convenience. It can
794 be found at https://www.youtube.com/playlist?list=PLI54dBkP-i2QjkHx10Z6FCmlDW_kZUAIX. It includes the videos as follows:

- 796 • <https://youtu.be/EdyDqvGr8ww> provides an overview of the various steps
797 involved into producing an X-ray image with our tool.
- 798 • <https://youtu.be/zitw5-Xk4dY> illustrates the character animation frame-
799 work and the real-time deformation of internal soft tissues.
- 800 • <https://youtu.be/1s-eTT1pCy8> provides evidence of motion capture using
801 the Microsoft Kinect to transfer the position of an actual human being to the
802 virtual patient.
- 803 • <https://youtu.be/EDJM3pSWtgo> focuses on the side markers.
- 804 • <https://youtu.be/x7KGsNSMSh8> focuses on digital image manipulation of
805 the produced X-ray image.
- 806 • <https://youtu.be/02K2ojcExTc> shows special cases (collapsed lung and the
807 insertion of foreign objects).
- 808 • <https://youtu.be/GwWY8AQffEY> shows that our tool can be extended to pro-
809 vide students with exercises.
- 810 • <https://youtu.be/WFOAVSLXufs> is a longer video, with a summary of the
811 most important functionalities of our tool.

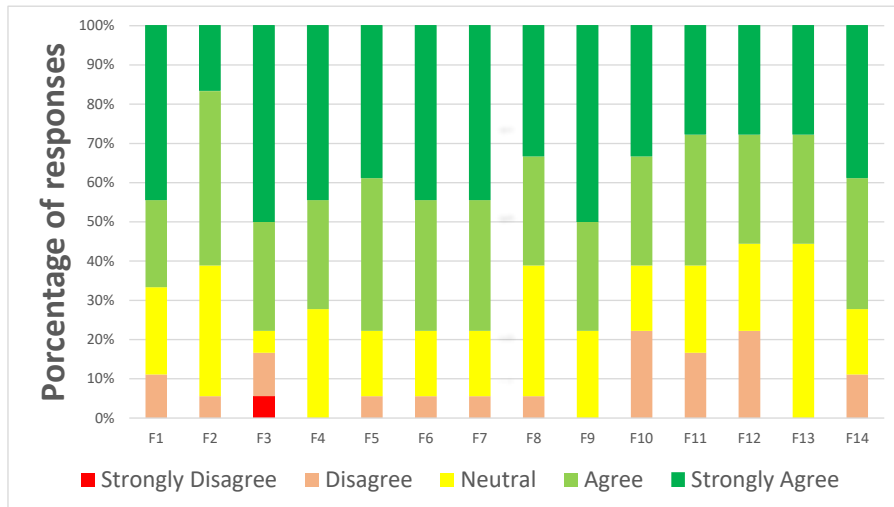


Figure 13: Likert scale responses of face validity.

Face validity	
F1:	The patient model before selecting the posing is visually realistic.
F2:	The deformation of the patient's internal anatomy is visually realistic.
F3:	The previously described steps characterize the procedure in a realistic way.
F4:	The placement of the side markers on the x-ray image is visually realistic.
F5:	The changes in the final x-ray image due to the adjustment of the beam direction and FRD are visually realistic.
F6:	The adjustment of the centre is visually realistic.
F7:	The changes in the final x-ray image due to the collimation adjustment are visually realistic.
F8:	The changes in the final x-ray image due to beam energy configuration are visually realistic.
F9:	In general, the changes in the final x-ray image due to modification of the different parameters are visually realistic.
F10:	The adjustment of the brightness and contrast settings is visually realistic.
F11:	The use of image filters is visually realistic.
F12:	The simulation of diseases is visually realistic.
F13:	The inclusion of foreign objects in the virtual patient is visually realistic.
F14:	Generally speaking, the simulator is visually realistic.

Table 2: Face validity questions

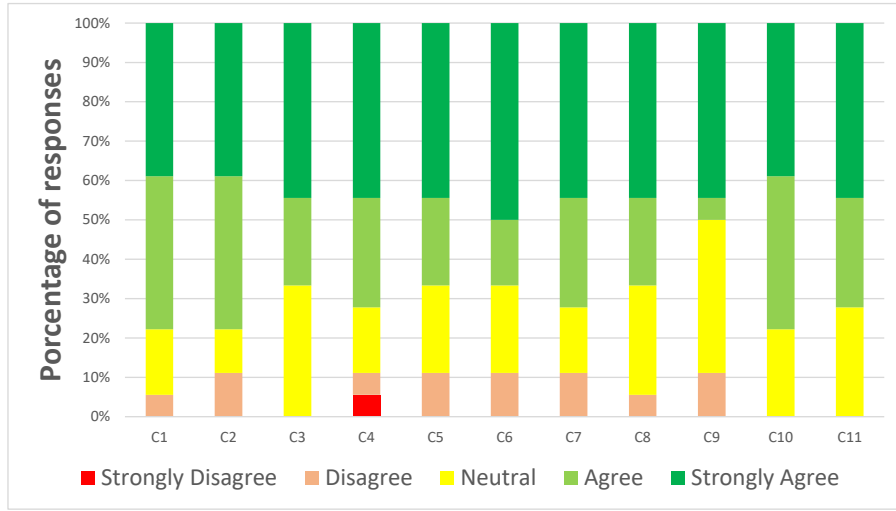
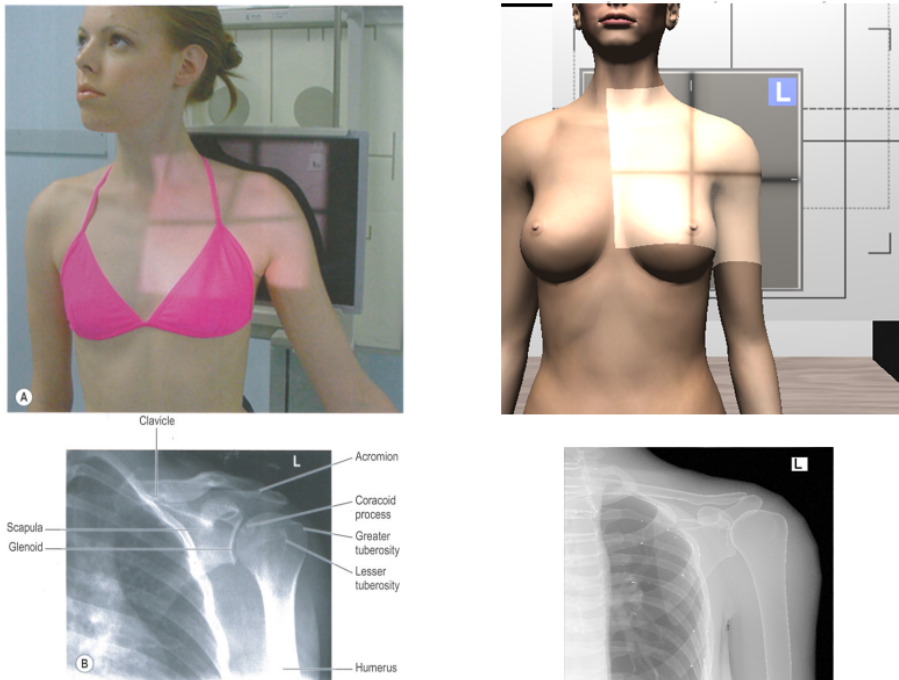


Figure 14: Likert scale responses of content validity.

Content validity	
C1:	Selecting the patient pose from a set of predefined ones is useful for self-guided training.
C2:	Selecting the patient manually is useful for self-guided training.
C3:	Selecting the patient pose from a set of predefined ones is useful to teach the procedure.
C4:	Selecting the patient manually is useful for teaching purposes (e.g. for live demonstration in the lecture theatre).
C5:	Regarding the previously described steps, the simulator is useful to teach the procedure.
C6:	Regarding the previously described steps, the simulator is useful for self-guided training.
C7:	In general, digital image manipulation of the X-ray image is useful for self-guided training and teaching.
C8:	Regarding the functionality described, this is useful to teach the procedure.
C9:	Regarding the functionality described, the simulator is useful for self-guided training.
C10:	Generally speaking, the simulator is suitable is useful as a teaching tool.
C11:	Generally speaking, the simulator is suitable for self-guided training.

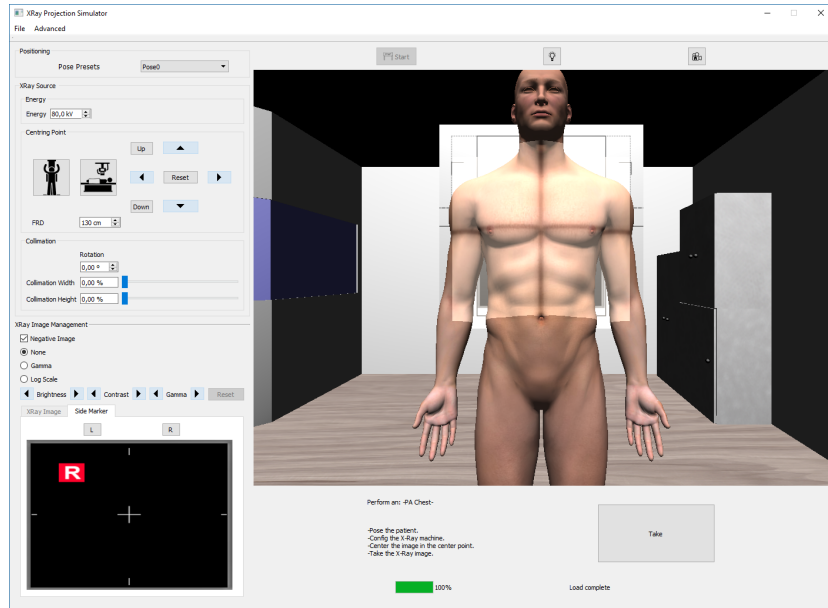
Table 3: Content validity questions



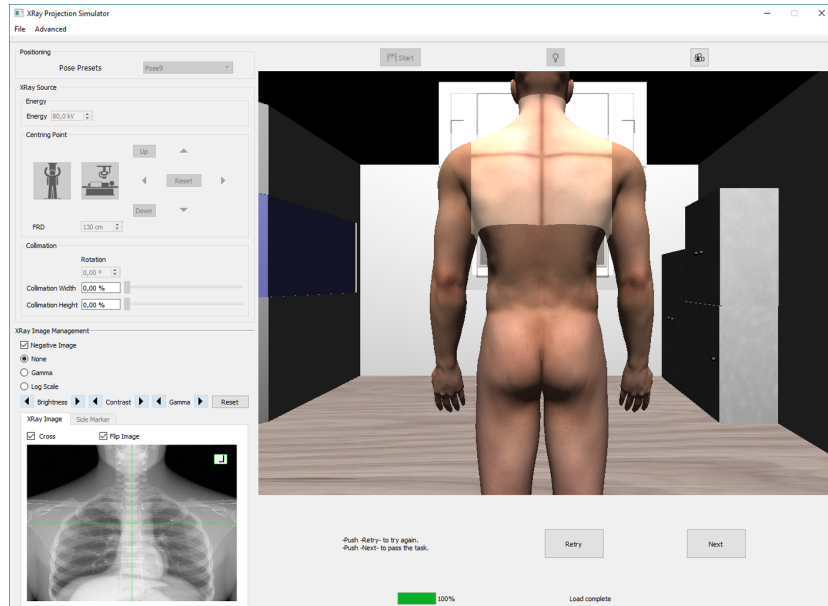
(a) Image courtesy of E. Carver, B. Carver and Elsevier Health Sciences [47].

(b) Projection replicated in the simulator.

Figure 15: Our system can replicate any type of projection, allowing the user to select the patient position and the X-ray configuration.



(a) Student must select a position without any hint and take a image without X-ray.



(b) Student can revise the result before next exercises.

Figure 16: GUI in non-guided training mode.